### Exact Floquet flat band and heating suppression via two-rate drive protocols

Tista Banerjee<sup>1</sup>, Sayan Choudhury<sup>2</sup>, and K. Sengupta<sup>1</sup>

<sup>1</sup>School of Physical Sciences, Indian Association for the Cultivation of Science, Jadavpur, Kolkata-700032, India.

<sup>2</sup>Harish Chandra Research Institute, A CI of Homi Bhabha National Institute,

Chhatnag Road, Jhunsi, Prayagraj, Uttar Pradesh 211019, India.

(Dated: April 11, 2024)

We demonstrate the existence of exact Floquet flat bands implying strong violation of the eigenstate thermalization hypothesis in a large class of closed quantum many-body systems in the presence of a two-rate drive characterized by frequencies  $\Omega_1$  and  $\Omega_2 = \nu \Omega_1$ . We provide the exact analytic condition for this phenomenon to occur for a generic protocol; in particular,  $\nu = (2p+1)$ , where p is an integer, leads to such flat bands for both square-pulse and cosine drive protocols for arbitrary  $\Omega_1$ . In the vicinity of these points, heating is suppressed up to very long timescales in such driven systems, leading to a prethermal regime; we demonstrate this by exact numerical studies of distribution and bandwidth of the Floquet eigenstates, spectral form factor, entanglement entropy, and correlation functions of an experimentally realizable finite driven Rydberg chain. The corresponding micromotion exhibits coherent reversal of excitation reminiscent of echoes. Our analysis constitutes a yet unexplored mechanism for heating suppression in driven closed quantum systems.

Eigenstate thermailzation hypothesis (ETH) forms the basis of our understanding of out-of-equilibrium behavior of a generic ergodic quantum system [1–4]. It predicts eventual thermalization of systems with initial states which are far from equilibrium consistent with the prediction of statistical mechanics. For a periodically driven system whose dynamics is governed by the Floquet Hamiltonian, such a steady state is characterized by infinite temperature [5]; the Floquet eigenstates for such a system has uniform probability distribution over the entire Floquet Brillouin zone (FBZ) leading to a bandwidth equal to the drive frequency.

The violation of ETH in quantum systems stems from the loss of ergodicity arising out of integrability [1], the presence of strong disorder [6], constraint induced fragmentation of its Hilbert space [7], or quantum scars [8, 9]. The Floquet analogue of such deviations have also been studied [10–12]; they typically occur in regimes of high drive amplitudes or frequencies and persist up to long prethermal timescales. However such effects are usually absent when the drive frequency becomes lower than or equal to typical system energy scales. In this regime, the thermalization is usually rapid and typically occurs over a few drive cycles.

Such rapid heating in driven quantum systems is detrimental to the coherent control of quantum devices for quantum state preparation and operations involving qubits; for example, dissipation is often used to counter heating effects in quantum state preparation [13, 14]. This has led to several suggestions for different drive protocols which minimizes heating such as counter-diabatic driving [15–17] or the method of optimal control [18]. However, to the best of our knowledge, neither of these methods have been successfully applied for reduction of heating in a generic driven non-integrable many-body system over long time scales.

In this work, we show that a two-rate periodic drive protocol [13, 19, 20] characterized by frequencies  $\Omega_1$  and  $\Omega_2 = \nu\Omega_1$ , where  $\nu$  is an integer, can lead to reduction of heating in a large class of non-integrable quantum many-body systems. We provide a generic condition where such a drive leads to ex-

act Floquet flat bands. For example, both square-pulse and cosine drive protocols with arbitrary  $\Omega_1$  and  $\nu = (2p+1)$  (where p denotes an integer) leads to relazation of these flat bands. In contrast to their counterparts studied in non-interacting driven models [21–23], these Floquet flat bands are exact, thereby constituting a strong violation of Floquet ETH. We also probe the characteristics of these driven systems around the parameter regime where flat bands occur; we find strong suppression of heating for a wide range of parameters and over large prethermal timescales in the intermediate and large drive frequency regimes. Moreover, the micromotion of such Floquet systems exhibit coherent reversal of excitations which is reminiscent of many-body echo protocols [24-26]. These properties lead to qualitative distinction of such driven systems from their single-rate counterparts. We provide a concrete example of this phenomenon using exact diagonalization (ED) on an experimentally realizable finite interacting Rydberg atom chain via study of its correlation functions, entanglement entropy, the distribution and bandwidth of its Floquet eigenstates, and the dynamics of the spectral form factor (SFF).

Exact Floquet Flat Bands: We consider a generic Hamiltonian driven by a two-rate protocol  $H(t) = \sum_{i=1,2} \lambda_i(t) \hat{O}_i$ . Here  $\lambda_i(t)$  are periodic functions of time with time period  $T_i = 2\pi/\Omega_i$  with  $i=1,2,\,\Omega_2 = \nu\Omega_1$ , and  $\hat{O}_i$  are generic many-body operators with  $[\hat{O}_1,\hat{O}_2] \neq 0$ . For integer  $\nu$ , the drive has a time period of  $T_1$ . The protocol chosen is schematically illustrated in Fig. 1(a). Importantly, the class of drive protocols chosen exhibits turning points at  $t_j = \beta_j T_1$  leading to  $\lambda_1(\alpha_j T_1) = 0 = \lambda_2(\alpha_j T_1)$  for  $\alpha_j = (\beta_{j+1} + \beta_j)/2$  as shown; this implies  $H(\alpha_j T_1) = 0$ . The two-rate generalization of several well-studied one-rate protocols meet this criteria. For instance, the square pulse protocol

$$\begin{array}{lll} \lambda_1(t) & = & +(-)\lambda_0 & \text{for } t \leq (>)T_1/2 \\ \\ \lambda_2(t) & = & w_0 - [+]w_1 \text{ for } \frac{(m-1)[m]T_1}{2\nu} \leq t < \frac{m[(m+1)]T_1}{2\nu} \end{array}$$

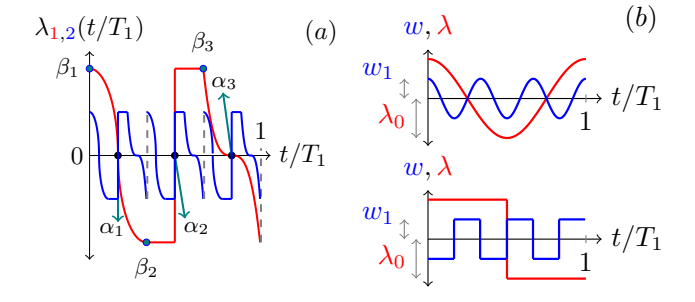


FIG. 1. (a) Schematic representation of the two-rate drive protocol studied in this work with  $\lambda_1(t/T_1)$  (red line) and  $\lambda_2(t/T_1)$  (blue line) for which  $H(t) = \lambda_1(t)\hat{O}_1 + \lambda_2(t)\hat{O}_2$  hosts Floquet flat bands. (b) Specific examples of the cosine (above, Eq. 2) and square-pulse (below, Eq. 1) protocols with  $\nu = 3$ ,  $\lambda_0 = 2w_1 = 1$  and  $w_0 = 0$ .

with  $w_0 = 0$ ,  $m = 1, 3, \dots 2\nu - 1$ , and  $\nu \in Z$  constitutes an example of such a protocol with  $\beta_1 = 0$  and  $\beta_2 = 1$  (see bottom panel of Fig. 1(b)). Similarly, the cosine protocol (top

panel of Fig. 1(b)) with

$$\lambda_1(t) = \lambda_0 \cos \Omega_1 t, \quad \lambda_2(t) = w_0 + w_1 \cos \nu \Omega_1 t \quad (2)$$

for  $\nu=2p+1$  with integer p and  $w_0=0$  is another example which corresponds to  $\beta_1=0,\ \beta_2=1/2$  and  $\beta_3=1$ . For both protocols,  $w_0$  serves as a tuning parameter which shall be used later to study the properties of the driven system near the perfect flat band limit.

As shown in Fig. 1, for  $w_0 = 0$ ,

$$\lambda_i(\alpha_i T_1 + t_0) = -\lambda_i(\alpha_i T_1 - t_0) \tag{3}$$

for all  $t_0 \leq (\beta_{j+1} - \beta_j)/2$ , so that  $H(\alpha_j T_1 + t_0) = -H(\alpha_j T_1 - t_0)$  for all  $\alpha_j$  and  $t_0$ . The evolution operator for such a drive protocol can be written as  $U(T_1,0) = \mathcal{T}_t \exp[-i\int^t dt' H(t')/\hbar]$ , where  $\mathcal{T}_t$  indicates time ordering. We write  $U(T_1,0)$  using Suzuki-Trotter decomposition and with time steps  $\Delta t = T_1/(N_0 + 1)$  so that

$$U(T_1, 0) = \prod_{k=1..N_0} e^{-iH(t_k)\Delta t/\hbar} = \prod_k U(t_{k+1}, t_k) = \prod_k U_k.$$

Next, we group  $U_k$ s between any two turning points  $\beta_j$  and  $\beta_{j+1}$  and reorganize the Trotter product for  $U(T_1, 0)$  to write

$$U(T_{1},0) = \prod_{j=j_{\text{max}}}^{1} U(\beta_{j+1}T_{1}, \beta_{j+1}T_{1} - \Delta t)U(\beta_{j+1}T_{1} - 2\Delta t, \beta_{j+1}T_{1} - \Delta t)...U(\alpha_{j}T_{1} + 2\Delta t, \alpha_{j}T_{1} + \Delta t)$$

$$\times U(\alpha_{j}T_{1}, \alpha_{j}T_{1} - \Delta t)...U(\beta_{j}T_{1} + 2\Delta t, \beta_{j}T_{1} + \Delta t)U(\beta_{j}T_{1} + \Delta t, \beta_{j})$$
(4)

where  $j_{\max}$  corresponds to the last turning point,  $\beta_{j_{\max}+1}=1$ , and we have used the fact that  $U(\alpha_jT_1+\Delta t,\alpha_jT_1)=I$  since  $H(\alpha_jT_1)=0$ . Noting that  $H(\alpha_jT_1+\Delta t)=-H(\alpha_jT_1-\Delta t)$  for any  $\alpha_j$ , we find that the terms in the first line Eq. 4 is the *exact Hermitian conjugate* of those in the second line. This leads to  $U(T_1,0)=I$  for such protocols. Since for any periodic drive  $U(T_1,0)=\exp[-iH_FT_1/\hbar]$ , this yields  $E_n^F(T_1)=0$  for all Floquet quasi-energies leading to an *exact flat band* for any  $\Omega_1$ . We note that such flat bands for a generic many-body Hamiltonian with non-commuting operators have no analogue for single rate drive protocols. These flat bands indicate complete localization of all Floquet quasienergies and therefore constitute a strong violation of the ETH which predicts an uniform distribution of Floquet eigenstates within the FBZ.

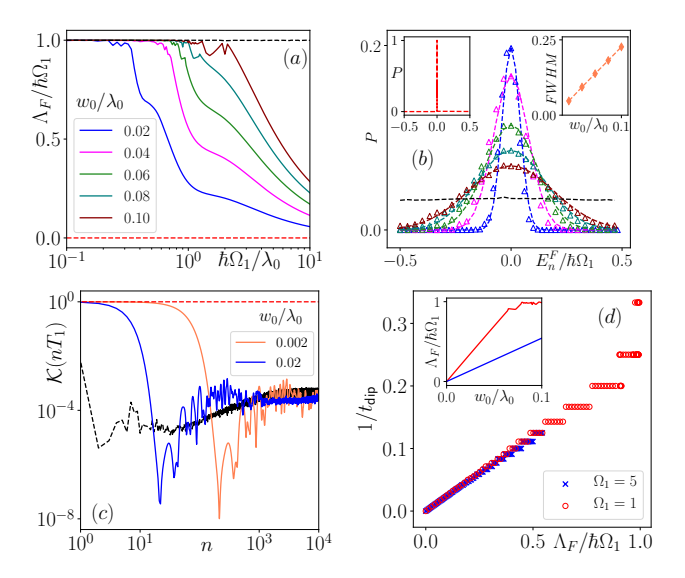
*Specific Model:* We now consider a specific non-integrable spin-model given by

$$H_R = \lambda_1(t) \sum_j \sigma_j^z + \lambda_2(t) \sum_j \tilde{\sigma}_j^x \tag{5}$$

where  $\sigma_j^{x,z}$  denotes Pauli matrices on site j, and  $\tilde{\sigma}_j^x = P_{j-1}\sigma_j^x P_{j+1}$ , where  $P_j = (1 - \sigma_j^z)/2$ . Such a model al-

lows spin-flip on site j only if the neighboring sites are in the spin-down state. It is well-known that this model describes the dynamics of a Rydberg atom array of length L in the so-called PXP limit [27, 28], with the Rydberg excitation density given by  $\hat{n}_j = (1+\sigma_j^z)/2$  and the detuning  $\Delta \equiv \lambda_1$ . In what follows, we are going to study the properties of this model in the presence of a two-rate drive protocols given by Eqs. 1 and 2 in a non-perturbative regime where the single-rate protocol exhibits rapid heating. The corresponding perturbative regime with  $\lambda_0 \gg \hbar\Omega_1, w_1, w_0$  is studied by analytical, albeit perturbative, techniques in the supplementary material [29].

Floquet Eigenstates: We use ED to obtain exact Floquet eigenvalues and eigenstates of  $H_R$  for the square-pulse protocol (Eq. 1); the details of the method and corresponding results for cosine protocol (Eq. 2) are presented in Ref. [29]. We first study the normalized Floquet bandwidth  $\Lambda_F/(\hbar\Omega_1)$  and the distribution of the Floquet eigenstates over the first FBZ  $(-1/2 \leq E_F^n/(\hbar\Omega_1) \leq 1/2)$  for several  $w_0$ . The results are shown in Fig. 2 (a) and (b) for several representative  $w_0/\lambda_0$  and  $w_1/\lambda_0=1$ . In this regime, a single-rate drive protocol with drive frequency  $\Omega_1$  and  $w_1=0$  exhibits  $\Lambda_F/(\hbar\Omega_1)=1$  for all  $\hbar\Omega_1/\lambda_0\leq 10$  as shown by the black dotted lines in Figs. 2(a); moreover the Floquet eigenvalues are almost uni-



formly distributed within the first FBZ as shown by the black curve in Fig. 2(b). These result are consistent with the prediction of ETH. In contrast, for the two-rate protocol with  $w_1/\lambda_0 = 1$ , we find a perfect flat band  $(\Lambda_F = 0)$  for all  $\Omega_1$  when  $w_0 = 0$  (red dotted line in Fig. 2(a)); the distribution of the eigenstates constitutes a delta-function at  ${\cal E}_n^{\cal F}=0$  (left inset of Fig. 2(b)). For finite  $w_0/\lambda_0$ ,  $\Lambda_F/\hbar\Omega_1 < 1$  for wide range of  $\Omega_1$  showing violation of ETH in a finite chain near the flat band limit. The distribution of  $E_n^F$ ,  $P(E_n^F/\hbar\Omega_1)\equiv P$ , is shown for representative  $w_0/\lambda_0$  in Fig. 2(b) for  $\hbar\Omega_1/\lambda_0=1$ ; the plot indicates that P is approximately Gaussian around  $E_n^F = 0$  indicating a deviation from the ETH prediction. The full width at half maxima (FWHM) of P increases linearly with  $w_0/\lambda_0$  for  $w_0 \ll \hbar\Omega_1$  (right inset of Fig. 2(b)); however, for the system sizes and frequency ranges studied here, it never reaches close to the ETH predicted uniform distribution.

Next, we analyze the SFF which is one of the key indicators of many-body quantum chaos for driven systems. The SFF corresponding to the Floquet eigenstates after n drive cycles

is determined by computing:

$$\mathcal{K}(nT_1) = \frac{1}{D^2} \sum_{p,q=1}^{D} e^{i(E_p^F - E_q^F)nT_1/\hbar}$$
 (6)

We note that in a driven ergodic system  $\mathcal{K}$  displays a characteristic dip-ramp-plateau structure at late times [30–32]. The occurrence of the first dip provides an estimate of the bandwidth, the position of the ramp indicates thermalization time, while the final plateau is expected to occur around the Heisenberg time  $t_H$  [33]. Fig. 2(c) shows a plot of  $\mathcal{K}$  as a function of n; the plot is obtained after averaging over  $n_0 = 100$  values of  $w_0$  obtained from an uniform distribution with  $\delta w_0 = 0.1 w_0$ . Such an averaging procedure is known to reduce oscillations in  $\mathcal{K}$  and are not otherwise central to our main results[30, 31, 33].

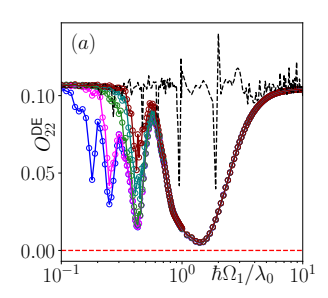
Fig. 2(c) shows that for  $\hbar\Omega_1=w_1=\lambda_0$ , the initial dip never occurs for  $w_0=0$  (red dashed line) while for the single rate drive protocol it occurs at  $n=n_d\simeq 1$ . An estimate of the dip time can be obtained by noting that at short times  $\mathcal{K}(nT_1)=1-(\epsilon_0nT_1)^2\sum_{p,q}(\epsilon_p^F-\epsilon_q^F)^2/\mathcal{D}^2$ . Here we have scaled all energies  $E_p^F/\epsilon_0=\epsilon_p^F$  and chosen  $\epsilon_0=\Lambda_F/\mathcal{D}$  to be an average level spacing. Converting the sum to an integral over energy gaps  $\epsilon$  with a corresponding density of states  $\rho(\epsilon/\Lambda_F)$ , we find

$$\mathcal{K}(nT_1) \simeq 1 - \frac{(\epsilon_0 n T_1)^2}{\hbar^2 \mathcal{D}} (\Lambda_F/\epsilon_0)^3 \int_{-1/2}^{1/2} dx \rho(x) x^2$$

$$= 1 - c_0 (n T_1 \Lambda_F/\hbar)^2 \tag{7}$$

where  $c_0$  is a constant whose precise value depends on system details. Eq. 7 therefore estimates a dip time  $t_{\rm dip}=n_dT_1$ , where  $n_d\sim {\rm Int}[\hbar/(T_1\Lambda_F)]$  and Int denotes the nearest integer. We find that  $t_{\rm dip}$  increases as one approaches the flat band limit; this is consistent with Fig. 2(d), where  $t_{\rm dip}^{-1}$  is plotted as a function of  $\Lambda_F/(\hbar\Omega_1)$ , demonstrating that  $t_{\rm dip}$  decreases with increasing  $\Lambda_F$ , which itself increases with  $w_0$  (as shown in the inset of Fig. 2(d)). The plateaus of  $t_{\rm dip}^{-1}$  seen in Fig. 2(d) occurs due to the integer nature of  $n_d$ ; a change in  $n_d$  requires a finite change in  $\Lambda_F$  and hence  $w_0$ . Since thermalization occurs after the dip in the SFF, these results show that tuning  $w_0$  can lead to a large prethermal timescale in these systems. This tunability has no analogue for single-rate protocols.

Correlation and Entanglement: It is well-known that typical local correlation functions for the finite Rydberg chain reaches the Floquet ETH predicted diagonal ensemble (DE) value. Here we study the DE value of the correlation function,  $O_{j2}^{\mathrm{DE}} = \mathrm{Tr}[\rho_D \hat{n}_j \hat{n}_{j+2}]$  starting the from the vacuum (all spin down) initial state. Here  $\rho_D$  denotes the density matrix corresponding to the diagonal ensemble for the square-pulse protocol [2];  $O_{j2}^{\mathrm{DE}}$  coincides with  $O_{j2}(nT_1) = \langle \psi(nT_1)|\hat{n}_j\hat{n}_{j+2}|\psi(nT_1)\rangle$  for  $n\to\infty$ . The plot  $O_{22}^{\mathrm{DE}}$  is shown in Fig. 3(a) as a function of the drive frequency  $\Omega_1$  for  $w_1/\lambda_0 = 1$  and  $\nu = 3$ . For the single-rate drive,  $O_{j2}^{\mathrm{DE}} \simeq 0.105$  as shown in black dashed line in Fig. 3(a)



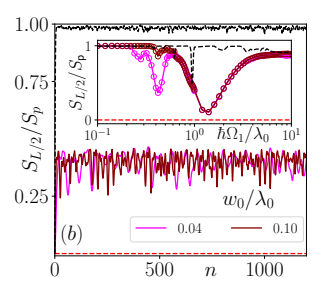
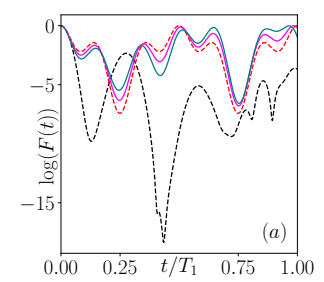


FIG. 3. (a) Plot of the diagonal ensemble value of the correlation function,  $O_{22}^{\mathrm{DE}}$  as a function of  $\hbar\Omega_1/\lambda_0$  for L=20 and several representative  $w_0/\lambda_0$ . The colors for different  $w_0$  are same as in Fig. 2(a). (b) Plot of  $S_{L/2}/S_p$  as a function of n for L=22,  $\hbar\Omega_1/\lambda_0=1$  and several  $w_0/\lambda_0$ . The inset shows a plot of long-time averaged value of  $S_{L/2}/S_p$  (averaged over 200 drive cycles around n=1100) as a function of  $\hbar\Omega_1/\lambda_0$  for several  $w_0/\lambda_0$ . For all plots  $w_1/\lambda_0=1$ . The black (red) dashed line corresponds to  $w_1/\lambda_0=0(1)$  and  $w_0/\lambda_0=1(0)$ . The drive used corresponds to the square-pulse protocol (Eq. 1) with  $\nu=3$ . See the section on Correlation and Entanglement for more details.

[11]; in contrast, for  $w_0=0$ ,  $O_{22}$  remain pinned to its initial zero value for all  $\Omega_1$  (red dashed line). In addition, for  $w_0/\lambda_0 \leq 0.1$  and  $0.5 \leq \hbar\Omega_1/\lambda_0 \leq 5$ , it exhibits a broad dip whose width is almost independent of  $w_0$  and remains below the ETH predicted value. This behavior is qualitatively different from that obtained from single rate drive; an analytical understanding of this feature for small system sizes is presented in the supplementary material [29].

A similar signature is found by studying the half-chain entanglement entropy  $S_{L/2}$  of the driven chain [11, 12]. We find that for  $w_0/\lambda_0 \leq 0.1$ ,  $S_{L/2}$  never reaches its Page value  $S_p$ [34] for  $n \leq 10^3$  cycles signifying the absence of an infinite temperature steady state. As shown in Fig. 3(b),  $S_{L/2}/S_p$ oscillates around an average  $\sim 0.27$  for  $\hbar\Omega_1/\lambda_0 = 1$  and  $0.02 \le w_0/\lambda_0 \le 0.1$ . This behavior is in sharp contrast to the single rate drive protocol where  $S_{L/2}$  reaches  $S_p$  within a few drive cycles (black dashed line in Fig. 3(b)). For  $w_0 = 0$ ,  $S_{L/2} = 0$  as expected in the perfect flat band limit (red dashed line in Fig. 3(b)). The inset shows the late-time behavior of  $S_{L/2}/S_p$  obtained by averaging over 200 cycles around n=1100; we find a similar dip as  $O_{22}^{DE}$ , showing lack of thermalization for all  $w_0/\lambda_0 \leq 0.1$  and  $0.5 \leq \hbar\Omega_1/\lambda_0 \leq 5$ . These results identify a wide range of  $\Omega_1$  and  $w_0$  around the flat band limit for which heating is significantly suppressed.

Floquet Micromotion: Up to now, we have examined the stroboscopic dynamics of the system. In order to completely characterize the dynamics of the system, we now proceed to examine the Floquet micromotion. We find that the micromotion for the two-rate drive protocol also exhbits a qualitatively different behavior compared to its single-rate counterpart. To understand this, we study the logarithm of the fidelity  $F(t) = |\langle \psi(0)|\psi(t)\rangle|^2$  and  $S_{L/2}(t)$  of such a driven chain using a cosine drive protocol (Eq. 2) and starting the from the all spin down (vacuum) initial state. A plot of F(t) and  $S_{L/2}(t)$ ,



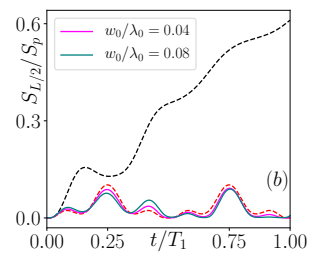


FIG. 4. Plot of (a) the logarithm of the fidelity,  $F(t) = |\langle \psi(0)|\psi(t)\rangle|^2$  and (b) the half-chain entanglement entropy (normalized by the Page value),  $S_{L/2}/S_p$  as a function of  $t/T_1$  ( $0 \le t/T_1 \le 1$ ) for  $w_1/\lambda_0 = 1$  and several representative  $w_0/\lambda_0$  showing coherent revival of excitation for the two-rate protocol during the micromotion. The black (red) dashed line corresponds to  $w_1/\lambda_0 = 0(1)$  and  $w_0/\lambda_0 = 1(0)$ . For all plots L = 20,  $\nu = 3$ ,  $\hbar\Omega_1/\lambda_0 = 1$  and the protocol used is the cosine drive given by Eq. 2.

shown in Figs. 4(a) and (b) for  $\hbar\Omega_1/\lambda_0=1=w_1/\lambda_0$  and for several representative  $w_0/\lambda_0$ , brings out this difference. We find that F(t) and  $S_{L/2}(t)$  for the two-rate protocol shows clear signature of coherent reversal of excitations representing an almost perfect echo [24, 25] as can be seen from their non-monotonic nature (Fig. 4); both of these quantities display oscillatory behavior close to their initial values for all  $w_0 \leq 0.1$ . These features indicate that the state of the driven system almost comes back to itself at  $t = T_1$ ; such an echo is exact in the flat-band limit ( $w_0 = 0$ ). In contrast, the single-rate drive protocol leads to strong decay of F(t) and fast growth of  $S_{L/2}(t)$  consistent with rapid spread of the initial state in the Hilbert space leading to rapid heating. Finally, we note that for the two-rate drive protocol, the micromotion displays a reflection symmetry around  $t = T_1/2$  for  $w_0 = 0$ :  $F(t) = F(T_1 - t)$  and  $S_{L/2}(t) = S_{L/2}(T_1 - t)$  for all  $t \le T_1$ . This is an exact symmetry of the dynamics in the flat-band limit for both cosine and square-pulse protocols [29].

Discussion: The two-rate protocols studied in this work provide a way to realize exact Floquet flat bands for a large class of ergodic driven Hamiltonians. It is well-known that flat bands provide a starting point for studying ultra-strong correlation; our work provides the first Floquet version of this phenomenon. Here we concentrate on the reduction of heating due to the presence of such flat bands and the resultant coherent reversal of excitation formation in the micromotion of such systems. We note that such a suppression of heating is beneficial for quantum state preparation and qubit manipulation in driven systems. We also expect our work to lead to several future extensions; for example introduction of disorder through  $w_0$  shall allow us to study aspects of Floquet MBL in such systems. It would also be interesting to examine protocols that use two-rate driving to engineer time-translationsymmetry-breaking, thereby realizing discrete time crystals. We intend to address these and other related issues in future

To conclude we have identified a class of two-rate drive pro-

tocols which allows one to realize exact Floquet flat bands leading to strong violation of ETH. We have identified a perturbative regime around the parameter regime leading to these flat bands where heating is strongly suppressed. Our study therefore provides an yet unexplored avenue to reduction of heating in driven quantum systems and is expected to have applications in quantum state preparation, quantum simulation, and quantum metrology.

Acknowledgement: KS thanks DST, India for support through SERB project JCB/2021/000030 and Arnab Sen for discussions. SC thanks DST, India for support through SERB project SRG/2023/002730. TB thanks Mainak Pal for discussions.

- [1] A. Polkovnikov, K. Sengupta, A. Silva, and M. Vengalattore, Rev. Mod. Phys., 83, 863 (2011); J. Dziarmaga, Adv. Phys. 59, 1063 (2010);
- [2] L. D'Alessio, Y. Kafri, A. Polkovnikov, and M. Rigol, Adv. Phys. 65, 239 (2016).
- [3] L. D'Alessio and A. Polkovnikov, Ann. Phys. 333, 19 (2013);
   M. Bukov, L. D'Alessio, and A. Polkovnikov, Adv. Phys. 64, 139 (2015).
- [4] M. Heyl, Rep. Prog. Phys 81, 054001 (2018); F. Harper, S. Roy, M. S. Rudner, and S. L. Sondhi, Annu. Rev. Condens. Matter Phys. 11, 345 (2020).
- [5] L. D'Alessio and M. Rigol, Phys. Rev. X 4, 041048 (2014).
- [6] R. Nandakishore and D. Huse, Ann. Rev. Cond. Mat 6, 15 (2015); D. A. Abanin, E. Altman, I. Bloch, and M. Serbyn Rev. Mod. Phys. 91, 021001 (2019);
- [7] S. Moudgalya, A. B. Bernavig, and N. Regnault, Rep. Prog. Phys. 85, 086501 (2022);
- [8] H. Bernien et al., Nature 551, 579 (2017); C. J. Turner, A. A. Michailidis, D. A. Abanin, M. Serbyn, and Z. Papić, Nat. Phys. 14, 745 (2018); S. Choi, C. J. Turner, H. Pichler, W. W. Ho, A. A. Michailidis, Z. Papić, M. Serbyn, M. D. Lukin, and D. A. Abanin, Phys. Rev. Lett. 122, 220603 (2019); W. W. Ho, S. Choi, H. Pichler, and M. D. Lukin, Phys. Rev. Lett. 122, 040603 (2019); A Chandran, T. Iadecola, V. Khemani, and R. Moessner, Ann. Rev. Cond. Mat. 14, 443 (2023).
- [9] D. Banerjee and A. Sen Phys. Rev. Lett. 126, 220601 (2021);
   I. Sau, P. Stornati, D. Banerjee, and A. Sen Phys. Rev. D 109, 034519 (2024);
   I. S. Biswas, D. Banerjee, and A. Sen SciPost Phys. 12, 148 (2022)
- [10] P. Ponte, Z. Papić, F. Huveneers, and D. A. Abanin, Phys. Rev. Lett. 114, 140401 (2015); L. Zhang, V. Khemani, and D. A. Huse Phys. Rev. B 94, 224202 (2016).
- [11] B. Mukherjee, S. Nandy, A. Sen, D. Sen, and K. Sengupta, Phys. Rev B 101, 245107 (2020); B. Mukherjee, A. Sen, D. Sen, and K. Sengupta, Phys. Rev B 102, 075123 (2020); S. Sugiura, T. Kuwahara, and K. Saito, Phys. Rev. Research 3, L012010 (2021).
- [12] S. Ghosh, I. Paul, and K. Sengupta, Phys. Rev. Lett. 130, 120401 (2023).
- [13] E. Torrontegui, S. Ibanez, S. Martinez-Garaot, M. Modugno, A. del Campo, D. Guery-Odelin, A. Ruschhaupt, X. Chen, and J. G. Muga, Advances in atomic, molecular and optical physics 62, 117 (2013); A. del Campo and K. Sengupta, Eur. Phys. J. Special Topics 224, 189 (2015).
- [14] F. Verstraete, M. M. Wolf, and J. I. Cirac, Nat. Phys. 5, 633 (2009); P. M. Harrington, E. J. Mueller, K. W, Murch, Nat. Rev.

- Phys. 4, 660 (2022).
- [15] M. V. Berry, J. Phys. A: Math. Theor. 42, 365303 (2009).
- [16] A. del Campo, M. M. Rams, and W. H. Zurek, Phys. Rev. Lett. 109, 115703 (2012); A. del Campo, T. W. B. Kibble, W. H. Zurek, J. Phys. Cond. Mat. 25, 404210 (2013).
- [17] D. Sels and A. Polkovnikov, Proc. Natl. Acad. Sci. U.S.A. 114, E3909 (2017); P. W. Claeys, M. Pandey, D. Sels, and A. Polkovnikov, Phys. Rev. Lett. 123, 090602 (2019); M. Bukov, D. Sels, and A. Polkovnikov, Phys. Rev. X 9, 011034 (2019).
- [18] M. Demirplak and S. A. Rice, J. Chem. Phys. A 107, 9937 (2003); *ibid*, J. Chem. Phys. B 109, 6838 (2005); L. T. Brady, C. L. Baldwin, A. Bapat, Y. Kharkov, and A. V. Gorshkov, Phys. Rev. Lett. 126, 070505 (2021); M. Ljubotina, B. Roos, D. A. Abanin, and M. Serbyn PRX Quantum 3, 030343 (2022); L. Beringer, M. Steinhuber, J. D. Urbina, K. Richter, S. Tomsovic, arXiv:2401.17744v1 (unpublished).
- [19] J. D. Sau and K. Sengupta, Phys. Rev. B 90, 104306 (2014).
- [20] U. Divakaran and K. Sengupta, Phys. Rev. B 90, 184303 (2014).
- [21] Yingyi Huang, Phys. Rev. B **108**, 165139 (2023).
- [22] C. B. Dag and A. Mitra, Phys. Rev. B 105, 245136 (2022).
- [23] L. J. Maczewsky, J. M. Zeuner, S. Nolte, and A. Szameit, Nat. Comm. 8, 13756 (2017); S. Mukherjee, A. Spracklen, M. Valiente, E. Andersson, P. Öhberg, N. Goldman, and R. R. Thomson, Nat. Comm. 8, 13918 (2017).
- [24] T. Engl, J. D. Urbina, K. Richter, and P. Schlagheck, Phys. Rev. A 98, 013630 (2018); Y-Y Chen, P. Zhang, W. Zheng, Z. Wu, and H. Zhai, Phys. Rev. A 102, 011301(R) (2020).
- [25] C. Lv, R. Zhang, and Q. Zhou, Phys. Rev. Lett. 125, 253002 (2020); C-Y Wang, arXiv:2312.11910 (unpublished).
- [26] N. Maskara, A. A. Michailidis, W. W. Ho, D. Bluvstein, S. Choi, M. D. Lukin, and M. Serbyn, Phys. Rev. Lett. 127, 090602 (2021); D. Bluvstein, A. Omran, H. Levine, A. Keesling, G. Semeghini, S. Ebadi, T. T. Wang, A. A. Michailidis, N. Maskara, W. W. Ho, S. Choi, M. Serbyn, M. Greiner, V. Vuletić, and M. D. Lukin, Science 371, 1355 (2021); C. Lyu, S. Choudhury, C. Lv, Y. Yan, and Q. Zhou, Phys. Rev. Res. 125, 253002 (2020).
- [27] W. Bakr, J. Gillen, A. Peng, S. Foelling, and M. Greiner, Nature (London) 462, 74 (2009); W. S. Bakr, A. Peng, M. E. Tai, R. Ma, J. Simon, J. I. Gillen, S. Folling, L. Pollet, and M. Greiner, Science 329, 547 (2010).
- [28] H. Bernien, S. Schwartz, A. Keesling, H. Levine, A. Omran, H. Pichler, S. Choi, A. S. Zibrov, M. Endres, M. Greiner, V. Vuletic, and M. D. Lukin, Nature (London) 551, 579 (2017); H. Levine, A. Keesling, A. Omran, H. Bernien, S. Schwartz, A. S. Zibrov, M. Endres, M. Greiner, V. Vuletic, and M. D. Lukin, Phys. Rev. Lett. 121, 123603 (2018).
- [29] See supplementary materials for details.
- [30] A. Chan, A. De Luca, and J. T. Chalker, Phys. Rev. Lett. 121, 060601 (2018); S. J. Garratt and J. T. Chalker, Phys. Rev. Lett. 127, 026802 (2021).
- [31] S. Moudgalya, A. Prem, D. A. Huse, and A. Chan, Phys. Rev. Res, 3, 023176 (2021); A. Chan, S. Shivam, D. A. Huse, and A. De Luca, Nat. Commun. 13, 7484 (2022); S. Shivam, A. De Luca, D. A. Huse, and A. Chan Phys. Rev. Lett. 130, 140403 (2023).
- [32] P. Kos, M. Ljubotina, and T. Prosen, Phys. Rev. X 8, 021062 (2018); B. Bertini, P. Kos, and T. Prosen, Phys. Rev. Lett. 121, 264101 (2018); A. Flack, B. Bertini, and T. Prosen, Phys. Rev. Res. 2, 043403 (2020).
- [33] A. del Campo, J. Molina-Vilaplana, and J. Sonner, Phys. Rev. D 95, 126008 (2017).
- [34] D. N. Page, Phys. Rev. Lett. 71, 1291 (1993); L. Vidmar and M. Rigol, Phys. Rev. Lett. 119, 220603 (2017).

# Supplementary Materials to Exact Floquet flat band and heating suppression via two-rate drive protocols

Tista Banerjee<sup>1</sup>, Sayan Choudhury<sup>2</sup>, and K. Sengupta<sup>1</sup>
<sup>1</sup>School of Physical Sciences, Indian Association for the Cultivation of Science, Jadavpur, Kolkata-700032, India.

<sup>2</sup>Harish Chandra Research Institute, A CI of Homi Bhabha National Institute,

Chhatnag Road, Jhunsi, Prayagraj, Uttar Pradesh 211019, India.

(Dated: April 11, 2024)

### ADDITIONAL NUMERICAL RESULTS

To supplement our results on the Floquet eigenstates in the main text, we first provide an analysis of the spectral statistics. To this end, we study the distribution P(r) of the renormalized level-spacing ratio  $r_n$  which is given, in terms of the Floquet level spacings  $\epsilon_n^F = E_{n+1}^F - E_n^F$ , by [1–3]

$$r_n = \operatorname{Min}[\epsilon_n^F, \epsilon_{n+1}^F] / \operatorname{Max}[\epsilon_n^F, \epsilon_{n+1}^F]$$
 (1)

It is well-known that  $P(r_n)$  obeys the circular orthogonal ensemble (COE) at low frequency with  $r=\langle r_n\rangle=\sum_{r_n}P(r_n)r_n\simeq 0.527$ ; for the present system, at high frequency where the effective Floquet Hamiltonian  $H_F\equiv H_{\rm PXP}=w_0\sum_j\tilde{\sigma}_j^x,\ r\sim 0.536$  and P(r) is well approximated by a Gaussian unitary ensemble (GUE). In the latter

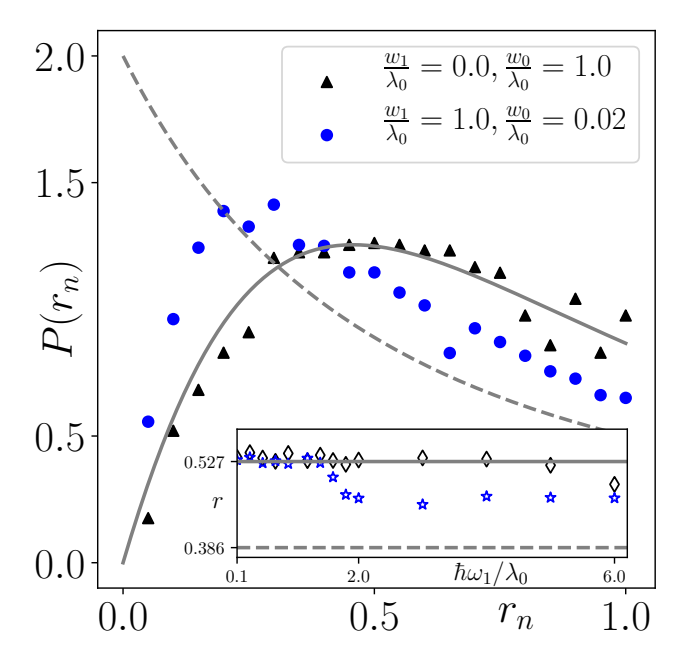


FIG. 1. Plot of  $P(r_n)$  as a function of  $r_n$  for the single-rate drive with  $w_0=1$  and  $w_1=0$  (black triangles) and the two-rate drive for  $w_0=0.02$  and  $w_1=1$  (blue circles) for  $\hbar\Omega_1=\lambda_0=1$ . The grey solid line corresponds to COE distribution while the grey dotted line indicates Poissonian statistics. The inset shows a plot of r as a function of  $\hbar\Omega_1/\lambda_0$  for both protocols. For all plots  $\nu=3$  and L=26 and we have considered eigenstates that belong to the zero total momentum  $(k_{\rm total}=0)$  and even parity (P=1) sector.

regime, the Floquet eigenvalues always remain within the first Floquet Brillouin zone (FBZ) and no unfolding is necessary. In contrast, in the former regime, majority of the eigenvalues need to be folded back in the first FBZ. In both these case, the states exhibits level repulsion leading to the respective ETH predicted value of r. However, for intermediate drive frequencies, only a finite fraction of the eigenvalues need to be folded back while the other stay within the first FBZ. Since the states which requires folding do not repel the unfolded ones [4], r deviates from its GUE or COE values and exhibits a dip at intermediate frequencies.

Fig. 1 where the black triangles (blue circles) correspond to the single-rate (two-rate) drive protocol with  $w_1=0$  and  $w_0=1$  ( $w_1=1$  and  $w_0=0.02$ ) and  $\hbar\Omega_1=\lambda_0=1$ , confirms this expectation. The plot of  $P(r_n)$  shows the expected COE feature for both drive protocols. However, for the two-rate drive protocol the peak of the distribution shifts to a lower value indicating lower value of r. This is confirmed in the inset where r is plotted as a function of  $\hbar\Omega_1/\lambda_0$ . We find a significant dip in r in the intermediate frequency regime  $2\hbar\Omega_1/\lambda_0 \le 5$  for the two-rate protocol where the single rate value is close to its COE predicted value; this feature is consistent with lower bandwidth of the spectrum leading to persistence of partial folding of Floquet eigenstates till a much lower frequency.

The reduction of heating for such two-rate drive protocols can be further understood from the dimensionless absorbed energy Q defined as [2]

$$Q = \frac{\langle \psi(nT) | H_F^{(1)} | \psi(nT) \rangle_{n \to \infty} - \langle H_F^{(1)} \rangle_{\infty}}{\langle H_F^{(1)} \rangle_{\infty} - \langle \psi(0) | H_F^{(1)} | \psi(0) \rangle}$$
(2)

where,  $\langle..\rangle_{\infty}$  denotes infinite-temperature average,  $H_F^{(1)}=\int_0^{T_1}H(t)dt/T_1$  is the average Hamiltonian which coincides with the exact  $H_F$  in the infinite frequency limit and is given by  $H_F^{(1)}=w_0\sum_j \tilde{\sigma}_j^x$ . Here we start from a superposition state  $|\psi(0)\rangle=\sum_n c_n|n\rangle$  where  $|n\rangle$  denotes Fock states with  $n\leq 3$  up-spins;  $c_n$ s are chosen so that the  $|\psi(0)\rangle$  corresponds to equal superposition of ten lowest bit representations (in the Fock basis starting from all spin-down state) of the  $k_{\rm total}=0$  momentum sector. This ensures that  $\langle \psi(0)|H_F^{(1)}|\psi(0)\rangle\neq 0$ . It is clear from the definition that  $-1\leq Q\leq 0$ ; the two limits correspond to its initial and infinite temperature values respectively. The plot of Q as a function of  $\hbar\Omega_1/\lambda_0$  is shown in Fig. 2; it clearly indicates that heating of the system is suppressed

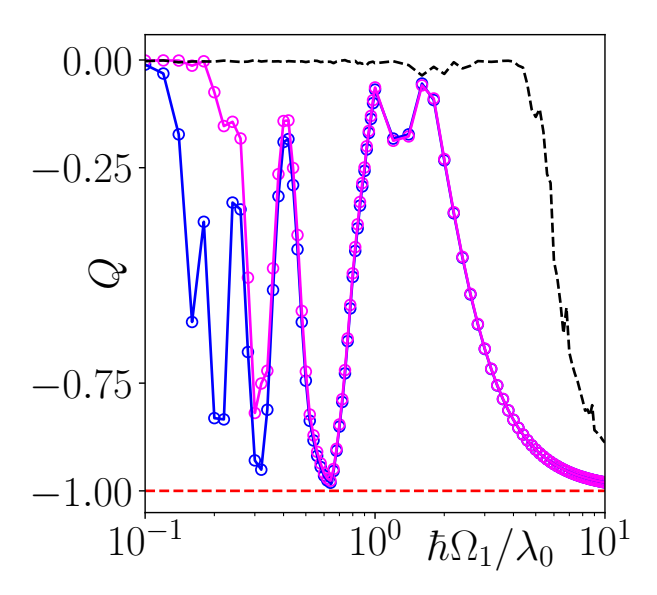


FIG. 2. Plot of Q as a function of  $\hbar\Omega_1/\lambda_0$  for the single-rate drive with  $w_0=1$  and  $w_1=0$  (black dashed line) and the two-rate drive for  $w_1/\lambda_0=1$  and several representative  $w_0/\lambda_0=0.04$  (pink circles) and 0.02 (blue circles) and 0 (red dashed line). For all curves r=3 and L=22.

for a finite chain in the presence of the two-rate protocol for all  $\hbar\Omega_1/\lambda_0 \geq 0.5$  and  $w_0 \leq 0.04$ . We have checked that qualitatively similar behavior occurs for all  $w_0 \leq 0.1$ . In this regime Q always remain negative indicating that the system does not heat up to infinite temperature; this is in sharp contrast to the single frequency drive as shown in Fig. 2.

The lack of heating in the presence of the two-rate drive protocol occurs due to the restricted spreading of the driven wavefunction in the Hilbert space. This can also be corroborated by studying the Shannon entropy. The Shannon entropy is given, in terms of the overlap

$$c_p^{q_0} = \langle p|q_0\rangle \tag{3}$$

of the exact Floquet eigenfunction  $|p\rangle$  with those  $(|q_0\rangle)$  of  $H_F^{(1)}$ , by

$$S_{\rm sh} = \sum_{p,q_0=1..\mathcal{D}} |c_p^{q_0}|^2 \ln |c_p^{q_0}|^2 / \mathcal{D}.$$
 (4)

It saturates to its circular ensemble value  $S_{\rm sh}^c \sim \ln 0.48 \mathcal{D}$  for an infinite temperature steady state and is zero when  $H_F^{(1)}$  coincides with  $H_F$ . A plot of  $S_{\rm sh}/S_{\rm sh}^c$ , shown in Fig. 3, as a function of frequency  $\hbar\Omega_1/\lambda_0$  indicates a much lower value compared to the single rate drive for a wide range of  $\Omega_1$  and for all  $w_0/\lambda_0 \leq 0.1$  indicating significantly lower spread in Hilbert space.

Next, we study the approach of the driven finite-sized chains to their thermodynamic limit. We note that the *perfect flat band limit* corresponds to a violation of ETH even in the thermodynamic limit. However, away from such fine

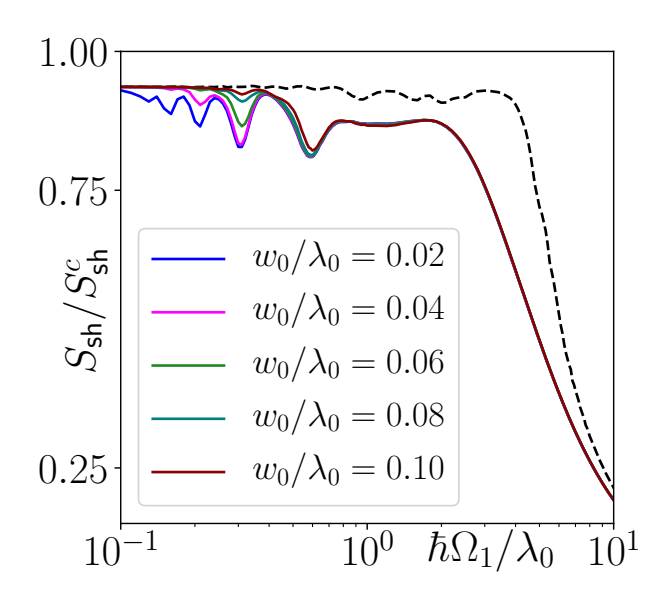


FIG. 3. Plot of  $S_{\rm sh}/S^c$  as a function of  $\hbar\Omega_1/\lambda_0$  for the single-rate drive with  $w_0=1$  and  $w_1=0$  (black dashed line) and the two-rate drive protocol with  $w_1/\lambda_0=1$  and several representative  $w_0/\lambda_0$ . For all plots  $\nu=3$  and L=20.

tuned points, *i.e.*, for any finite  $w_0$ , such driven systems are expected to ultimately converge to the ETH predicted infinite temperature results as  $L \to \infty$ . To verify this and to understand how fast the system approach this limit, we carry out a extrapolation of  $\Lambda_F/(\hbar\Omega_1)$  as shown in the inset of Fig. 4 for  $\hbar\Omega_1/\lambda_0=w_1/\lambda_0=1$  and  $w_0/\lambda_0=0.1$ . This allows us to extract a system size  $L^*$  beyond which  $\Lambda_F\sim\hbar\Omega_1$  which is the ETH predicted value. A plot of  $L^*$  as a function of  $\hbar\Omega_1/\lambda_0$  is shown in Fig. 4; we find that  $L^*$  is generically larger for the two-rate drive protocol at any  $\Omega_1$ . Moreover, it increases with decreasing  $w_0$ ; these features allow one to identify a parameter regime where a clear reduction of heating can be achieved for finite size systems.

Finally, we present exact numerical results for the distribution of the Floquet eigenstate,  $P(E_n/\hbar\Omega_1)\equiv P$  for cosine protocol with  $r=2,3,\ w_0/\lambda_0=0.04,\ w_1/\lambda_0=1$ , and  $\hbar\Omega_1/\lambda_0=1$  (see Eq. 2 of the main text) in Fig. 5. The corresponding inset shows a plot of the normalized Floquet bandwidth  $\Lambda_F/(\hbar\Omega_1)$  as a function of the drive frequency  $\hbar\Omega_1/\lambda_0$ . The plots of P for r=3 are qualitatively similar to their square-pulse counterpart discussed in the main text. In contrast, for r=2, where  $w_1=0$  does not lead to a flat band, P is almost flat; moreover  $\Lambda_F$  converges to the expected value  $\hbar\Omega_1$  quite fast. These features are qualitatively similar to the single drive protocol. These differences show the qualitative distinction between the dynamics obtained for odd integer values of r where  $w_1=0$  yield exact flat bands with their even integer counterparts.

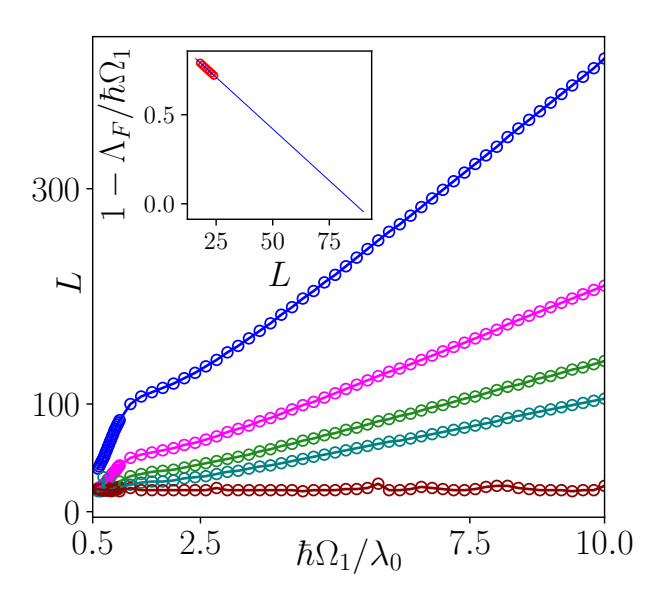


FIG. 4. Plot of  $L^*$  as a function of  $\hbar\Omega_1/\lambda_0$  for several  $w_0/\lambda_0$  and  $w_1/\lambda_0=1$ . The inset shows a plot of  $1-\Lambda_F/(\hbar\Omega_1)$  as a function of L for  $w_0/\lambda_0=0.02$ ;  $L^*$  is obtained from extrapolation of such plots such that  $\Lambda_F/(\hbar\Omega_1)=1$  for  $L=L^*$ .

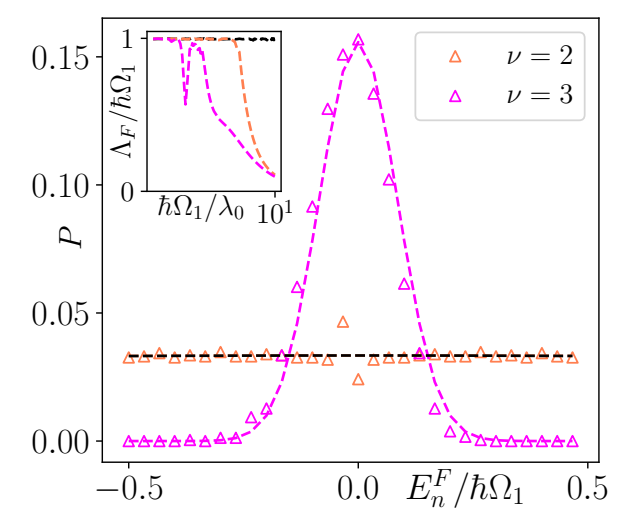


FIG. 5. Plot of the distribution P for r=2 (orange triangles) and r=3 (pink triangles) with  $w_0/\lambda_0=0.04$ ,  $w_1/\lambda_0=1$ , and  $\hbar\Omega_1/\lambda_0=1$ . The black dashed line correspond to a single rate protocol with  $w_0/\lambda_0=1$  and  $w_1=0$ . The eigenvalues were obtained by decomposing U(T,0) into  $N_0=500$  Trotter steps, followed by their diagonalization. A further increase in Trotter steps did not lead to significant change in the obtained eigenvalues. The inset shows a plot of  $\Lambda_F/(\hbar\Omega_1)$  as a function of  $\hbar\Omega_1/\lambda_0$ . For all plots, L=24. See text for details.

## FLOQUET HAMILTONIAN AT LARGE DRIVE AMPLITUDE

In this section, we are going to present analytic, albeit perturbative, results for the Floquet Hamiltonian for the case where amplitude of one of the drives is large:  $\lambda_0 \gg w_0, w_1$ . In this regime, once can use the standard Floquet perturbation theory (FPT) to obtain the Floquet Hamiltonian [5–7]. In what follows, we shall consider a square-pulse protocol for r=3 (Eq. 1 of the main text).

In the large drive amplitude regime, the Hamiltonian can be written as  $H=H_0(t)+H_1(t)$  where

$$H_0(t) = \lambda(t) \sum_j \sigma_j^z$$

$$H_1(t) = H_1^+ + H_1^-, \quad H_1^{\pm} = (w_0 + w_1(t)) \sum_j \tilde{\sigma}_j^{\pm}$$
(5)

Within the FPT, the zeroth order Floquet Hamiltonian is given by

$$U_{0}(t,0) = e^{-i\lambda_{0}t\sum_{j}\sigma_{j}^{z}/\hbar}\theta(T_{1}/2 - t) + e^{-i\lambda_{0}(T_{1}-t)\sum_{j}\sigma_{j}^{z}/\hbar}\theta(t - T_{1}/2)$$
 (6)

Since  $U_0(T_1,0)=I$ , this leads to  $H_F^{(0)}=0$ . To obtain the first-order term, we first define Fock states  $|m\rangle$  with m additional up-spins; note that  $|m\rangle$  corresponds to multiple Fock states since they may have different positions of these spins. To compute the first order Floquet Hamiltonian, we consider the matrix element of  $U_1(T_1,0)$  between these states. We first note that

$$U_1(T_1,0) = \sum_{s-+} \left(\frac{-i}{\hbar}\right) \int_0^{T_1} U_0^{\dagger}(t,0) H_1^s(t) U_0(t,0)$$
 (7)

and define integrals

$$I_{1}(t_{1}, t_{2}, s) = \int_{t_{1}}^{t_{2}} dt' e^{-2i\lambda_{0}st'/\hbar}$$

$$I_{2}(t_{1}, t_{2}, s) = \int_{t_{1}}^{t_{2}} dt' e^{-2i\lambda_{0}s(T_{1} - t')/\hbar}$$
(8)
(9)

where  $s=\pm 1.$  Using Eqs. 7 and 8, a few lines of straightforward algebra yields

$$\langle m|U_{1}(T_{1},0)|n\rangle = \left(\frac{-i}{\hbar}\right) \sum_{m,n,s=\pm 1} \delta_{m,n+s} c_{s}^{(1)}$$

$$c_{s}^{(1)} = \int_{0}^{T_{1}/2} dt' e^{-2i\lambda_{0}st'/\hbar} (w_{0} + w_{1}(t))$$

$$+ \int_{T_{1}/2}^{T_{1}} dt' e^{-2i\lambda_{0}s(T_{1}-t')/\hbar} (w_{0} + w_{1}(t'))$$
(10)

For r=3, the evaluation of the integrals need to be done by

further subdivision of the integrals into time intervals of T/6.

A straightforward computation yields

$$c_s^{(1)} = (w_0 - w_1)[I_1(0, T_1/6, s) + I_1(T_1/3, T_1/2, s) + I_2(5T_1/6, 2T_1/3, s)] + (w_0 + w_1)[I_1(T_1/6, T_1/3, s) + I_2(T_1/2, 5T_1/6, s) + I_2(2T_1/3, T_1, s)]$$
(11)

These integrals are straightforward to evaluate and leads to the final expression for  $U_1(T,0)$  to be

$$U_{1}(T,0) = \left(\frac{-iT_{1}}{\hbar}\right) \frac{w_{0} \sin(\lambda_{0} T_{1}/2)}{\lambda_{0} T_{1}/2} \sum_{j,s=\pm} \tilde{\sigma}_{j}^{s} e^{-i\lambda_{0} T_{1} s/2}$$
(12)

This yields the first order Floquet Hamiltonian  $H_F^{(1)}=(i\hbar/T)U_1(T,0)$  to be

$$H_F^{(1)} = \frac{w_0 \sin(\lambda_0 T_1/2)}{\lambda_0 T_1/2} \sum_{j,s=\pm} \tilde{\sigma}_j^s e^{-i\lambda_0 T_1 s/2}$$
 (13)

The Floquet hamiltonian yields flat bands for  $w_0=0$  for all  $T_1$ . In addition, as shown in Ref. [8], it shows approximate flat bands at first order for  $\lambda_0 T_1=2n\pi$  where  $n\in Z$  similar to the single-rate protocol studied earlier.

In the single rate protocol studied earlier,  $H_F$  only had odd-

order terms in  $w_0$ . This originated from the presence of the operator  $C_0 = \prod_j \sigma_j^z$  which satisfied  $QUQ^{-1} = U^{-1}$  leading to the requirement  $\{H_F,Q\} = 0$ . This necessitated that  $H_F$  have only terms which are product of odd numbers of  $\sigma_j^\pm$ ; thus only odd order terms (of  $w_0$ ) contributed to  $H_F$ . However for the present case when both  $w_0$  and  $w_1$  are finite, it is easy to check that  $QUQ^{-1} \neq U^{-1}$ . This leads to an asymmetry of the spectrum around  $E_F = 0$  and also allows for the second-order terms in  $H_F$  which we now proceed to compute.

To this end, we first compute  $U_2(T,0)$  given by

$$U_{2}(T_{1},0) = \sum_{s_{1},s_{2}=\pm} \left(\frac{-i}{\hbar}\right)^{2} \int_{0}^{T_{1}} dt_{1} U_{0}^{\dagger}(t_{1},0) H_{1}^{s_{1}}(t_{1}) (14)$$
$$\times U_{0}(t_{1},0) \int_{0}^{t_{1}} dt_{2} U_{0}^{\dagger}(t_{2},0) H_{1}^{s_{2}}(t_{2}) U_{0}(t_{2},0).$$

The matrix elements of  $U_2$  between the states  $|m\rangle$  and  $|n\rangle$  can be similarly computed and yields

$$\langle m|U_{2}(T_{1},0)|n\rangle = \left(\frac{-i}{\hbar}\right)^{2} \sum_{s_{1},s_{2}=\pm 1} c_{s_{1},s_{2}}^{(2)} \delta_{m,n+s_{1}+s_{2}}$$

$$c_{s_{1}s_{2}} = A_{1}(T_{1}/2,s_{1},s_{2}) + A_{2}(T,s_{1},s_{2}) + A_{3}(T_{1},s_{1})A_{4}(T_{1}/2,s_{2})$$

$$A_{1}(T_{1}/2,s_{1},s_{2}) = \int_{0}^{T_{1}/2} dt_{1}e^{-2i\lambda_{0}t_{1}s_{1}/\hbar} (w_{0}+w_{1}(t_{1})) \int_{0}^{t_{1}} dt_{2}e^{-2i\lambda_{0}t_{2}s_{2}/\hbar} (w_{0}+w_{1}(t_{2}))$$

$$A_{2}(T_{1},s_{1},s_{2}) = \int_{T_{1}/2}^{T_{1}} dt_{1}e^{-2i\lambda_{0}(T_{1}-t_{1})s_{1}/\hbar} (w_{0}+w_{1}(t_{1})) \int_{T_{1}/2}^{t_{1}} dt_{2}e^{-2i\lambda_{0}(T_{1}-t_{2})s_{2}/\hbar} (w_{0}+w_{1}(t_{2}))$$

$$A_{3}(T_{1},s_{1}) = \int_{T_{1}/2}^{T_{1}} dt_{1}e^{-2i\lambda_{0}(T_{1}-t_{1})s_{1}/\hbar} (w_{0}+w_{1}(t_{1})) \quad A_{4}(T_{1}/2,s_{2}) = \int_{0}^{T_{1}/2} dt_{1}e^{-2i\lambda_{0}t_{1}s_{2}/\hbar} (w_{0}+w_{1}(t_{1}))$$

$$(15)$$

To evaluate these integrals, we first consider  $A_1$ . To do this

one needs to evaluate  $w_1(t_1)$  and  $w_1(t_2)$  at each time step. This leads to the result

$$A_{1}(T_{1}/2, s_{1}, s_{2}) = (w_{0} - w_{1})^{2}(L_{1} + L_{4} + L_{6}) + (w_{0}^{2} - w_{1}^{2})(L_{2} + L_{5}) + (w_{0} + w_{1})^{2}L_{3}$$

$$A_{2}(T_{1}, s_{1}, s_{2}) = (w_{0} + w_{1})^{2}(L'_{1} + L'_{4} + L'_{6}) + (w_{0}^{2} - w_{1}^{2})(L'_{2} + L'_{5}) + (w_{0} - w_{1})^{2}L'_{3}$$

$$A_{3}(T_{1}, s_{1}) = (w_{0} - w_{1})I_{2}(5T_{1}/6, 2T_{1}/3, s_{2}) + (w_{0} + w_{1})[I_{2}(T_{1}/2, 5T_{1}/6, s_{2}) + I_{2}(2T_{1}/3, T_{1}, s_{2})]$$

$$A_{4}(T_{1}/2, s_{1}) = (w_{0} + w_{1})I_{1}(T_{1}/6, T_{1}/3, s_{1}) + (w_{0} - w_{1})[I_{1}(0, T_{1}/6, s_{1}) + I_{1}(T_{1}/3, T_{1}/2, s_{1})]$$

$$(16)$$

The expressions for  $A_3$  and  $A_4$  in Eq. 16 can be obtained in

terms of the integrals  $I_1$  and  $I_2$  defined in Eq. 8. In contrast,

which are given by

$$L_{1} = \int_{0}^{T_{1}/2} dt_{1} e^{-2i\lambda_{0}s_{1}t_{1}/\hbar} \int_{0}^{t_{1}} dt_{2} e^{-2i\lambda_{0}s_{2}t_{2}/\hbar}, \quad L_{1}' = \int_{T_{1}/2}^{T_{1}} dt_{1} e^{-2i\lambda_{0}s_{1}(T_{1}-t_{1})/\hbar} \int_{T_{1}/2}^{t_{1}} dt_{2} e^{-2i\lambda_{0}s_{2}(T_{1}-t_{2})/\hbar} \\ L_{2} = \int_{T_{1}/6}^{T_{1}/2} dt_{1} e^{-2i\lambda_{0}s_{1}t_{1}/\hbar} \int_{0}^{T_{1}/6} dt_{2} e^{-2i\lambda_{0}s_{2}t_{2}/\hbar}, \quad L_{2}' = \int_{2T_{1}/3}^{T_{1}} dt_{1} e^{-2i\lambda_{0}s_{1}(T_{1}-t_{1})/\hbar} \int_{T_{1}/2}^{2T_{1}/3} dt_{2} e^{-2i\lambda_{0}s_{2}(T_{1}-t_{2})/\hbar} \\ L_{3} = \int_{T_{1}/6}^{T_{1}/2} dt_{1} e^{-2i\lambda_{0}s_{1}t_{1}/\hbar} \int_{T_{1}/6}^{t_{1}} dt_{2} e^{-2i\lambda_{0}s_{2}t_{2}/\hbar}, \quad L_{3}' = \int_{2T_{1}/3}^{T_{1}} dt_{1} e^{-2i\lambda_{0}s_{1}(T_{1}-t_{1})/\hbar} \int_{2T_{1}/3}^{t_{1}} dt_{2} e^{-2i\lambda_{0}s_{2}(T_{1}-t_{2})/\hbar} \\ L_{4} = \int_{T_{1}/3}^{T_{1}/2} dt_{1} e^{-2i\lambda_{0}s_{1}t_{1}/\hbar} \int_{0}^{T_{1}/6} dt_{2} e^{-2i\lambda_{0}s_{2}t_{2}/\hbar}, \quad L_{4}' = \int_{5T_{1}/6}^{T_{1}} dt_{1} e^{-2i\lambda_{0}s_{1}(T_{1}-t_{1})/\hbar} \int_{T_{1}/2}^{2T_{1}/3} dt_{2} e^{-2i\lambda_{0}s_{2}(T_{1}-t_{2})/\hbar} \\ L_{5} = \int_{T_{1}/3}^{T_{1}/2} dt_{1} e^{-2i\lambda_{0}s_{1}t_{1}/\hbar} \int_{T_{1}/6}^{t_{1}} dt_{2} e^{-2i\lambda_{0}s_{2}t_{2}/\hbar}, \quad L_{5}' = \int_{5T_{1}/6}^{T_{1}} dt_{1} e^{-2i\lambda_{0}s_{1}(T_{1}-t_{1})/\hbar} \int_{2T_{1}/3}^{t_{1}} dt_{2} e^{-2i\lambda_{0}s_{2}(T_{1}-t_{2})/\hbar} \\ L_{6} = \int_{T_{1}/3}^{T_{1}/2} dt_{1} e^{-2i\lambda_{0}s_{1}t_{1}/\hbar} \int_{T_{1}/3}^{t_{1}} dt_{2} e^{-2i\lambda_{0}s_{2}t_{2}/\hbar}, \quad L_{6}' = \int_{5T_{1}/6}^{T_{1}} dt_{1} e^{-2i\lambda_{0}s_{1}(T_{1}-t_{1})/\hbar} \int_{5T_{1}/6}^{t_{1}} dt_{2} e^{-2i\lambda_{0}s_{2}(T_{1}-t_{2})/\hbar} (17)$$

The evaluation of these integrals are tedious but straightforward. These lead to the expressions of  $c_{s_1,s_2}^{(2)}$  and  $U_2(T_1,0)$  can be expressed as

$$U_2(T_1,0) = \left(\frac{-i}{\hbar}\right)^2 \sum_{j_1,j_2} c_{s_1,s_2}^{(2)} \sigma_{j_1}^{s_1} \sigma_{j_2}^{s_2}$$

$$H_F^{(2)} = \left(\frac{i\hbar}{T_1}\right) \left(U_2(T_1,0) - U_1(T_1,0)^2/2\right) \tag{18}$$

where  $U_1(T_1,0)$  is given by Eq. 12.

While evaluating  $H_F^{(2)}$  using Eq. 18 we find that it vanishes if  $s_1=s_2$ . Moreover it also vanishes if  $j_1\neq j_2$  or  $j_1\neq j_2\pm 1$ . The last property ensures locality of the Floquet Hamiltonian. Furthermore we note that terms such as  $\tilde{\sigma}_j^-\sigma_{j'}^+$  is identically zero for  $j\neq j'$  due to the constraint on the spins. Finally, we find that  $H_F^{(2)}=0$  if either  $w_0=0$  or  $w_1=0$ ; this ensures that our results are consistent with both the exact flat band limit  $(w_0=0)$  and the single rate drive protocol  $(w_1=0)$  where  $H_F^{(2)}$  is known to vanish. A straightforward but somewhat cumbersome algebra, using Eqs. 16, and 17 yields

$$H_F^{(2)} = \frac{2w_0w_1\mathcal{C}}{\lambda_0} \sum_j \left( \sigma_j^z + (\tilde{\sigma}_j^+ \tilde{\sigma}_{j+1}^- + \text{h.c.}) \right)$$

$$\mathcal{C} = 6(2\sin x/6 - 2\sin x/3 + \sin x/2)/x - 1,(19)$$

where  $x = 2\lambda_0 T_1/\hbar$ . Note that in the high frequency limit where  $x \to 0$ ,  $C(x) \to 0$  which is consistent with standard high-frequency Magnus expansion.

A comparison between the distribution of eigenstates,  $P(E_n) \equiv P$ , of the analytical Floquet Hamiltonian  $H_F^{\rm an} = H_F^{(1)} + H_F^{(2)}$  and the exact Floquet Hamiltonian  $H_F^{\rm exact}$  obtained using ED is shown in Fig. 6 for  $\hbar\Omega_1/w_0 = 15$ ,  $w_1/w_0 = 0.1$ , and  $\lambda_0/w_0 = 20$ . The result indicates excel-

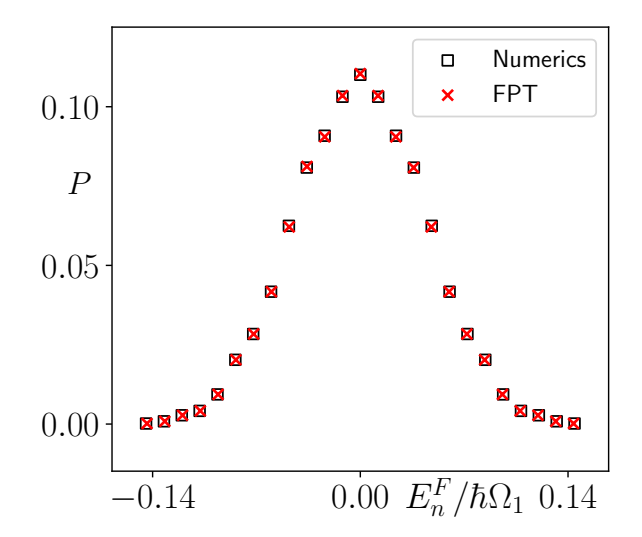


FIG. 6. Plot of the eigenvalue distribution P within the first FBZ for  $\hbar\Omega_1/w_0=15,\,w_1/w_0=0.1,\,$  and  $\lambda_0/w_0=20.$  The red crosses show results from second order FPT while the black open squares indicate those from exact numerics obtained using ED. For both plots we have used square pulse protocol and L=18.

lent match between the exact numerics and the second-order Floquet theory demonstrating that the Floquet eigenvalues are accurately captured in the large drive amplitude regime by the FPT.

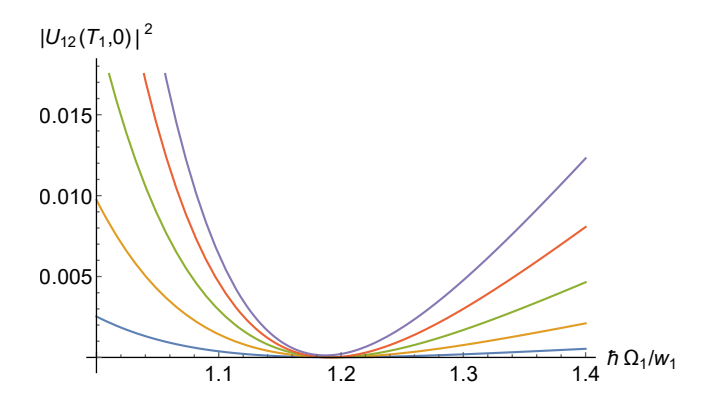


FIG. 7. Plot of  $|U_{12}(T_1,0)|^2$  as a function of  $\hbar\Omega_1/w_1$  for  $w_0=0.02..01$  (bottom to top curves in steps of 0.02).

### APPROXIMATE FREEZING FOR L=3

The phenomenon of dynamic freezing at special drive frequencies starting from the vacuum (all spin-down state) was

studied for the single-rate drive protocol in Ref. [9]. An analytical insight into the problem was obtained by studying the L=3 system analytically. Here we shall carry out a similar study for the two-rate protocol and aim to obtain an analytic understanding of the wide dip in  $O_{22}^{\rm DE}$  discussed in the main text. To this end, we note that for the L=3 in the k=0 sector, there are just two states given by  $|\phi_0\rangle=|\downarrow,\downarrow,\downarrow\rangle$  and  $|\phi_1\rangle=(|\uparrow,\downarrow,\downarrow\rangle+|\downarrow,\uparrow,\downarrow\rangle+|\downarrow,\downarrow,\uparrow\rangle)/\sqrt{3}$ . In the space of these two states, one can define a  $2\times 2$  matrix Hamiltonian given by

$$A(s_1, s_2) = s_1 \lambda_0 (1 - \tau_z) / 2 + (w_0 + w_1 s_2) \tau_x$$
 (20)

where  $s_{1,2} = \pm 1$ . The evolution operator for the square-pulse protocol given by Eq. (1) of the main text can then be written

$$U(T_1,0) = e^{-iA(-1,-1)T_1/(6\hbar)}e^{-iA(-1,1)T_1/(6\hbar)}e^{-iA(-1,-1)T_1/(6\hbar)}e^{-iA(1,1)T_1/(6\hbar)}e^{-iA(1$$

The time evolution any local operator, starting from  $|\phi_0\rangle$  is therefore controlled by  $U_{12}(T_1,0)$  which we study as function

of  $\Omega_1$ . For general  $w_0$  and  $w_1$ , the expression of  $U_{12}(T_1, 0)$  is cumbersome. However, its expression for the case  $w_0 = w_1$  is particularly simple and is given by

$$U_{12}(T_1,0) = (2i\sqrt{3}e^{-ix}\sin y)(z^2 - 12i\sin 2x + 2e^{-ix}\cos 2x((z^2 + 6(e^{2ix} - 1))\cos 2y - iz\lambda_0\sin 2y))/z^3$$
 (22)

where all quantities are scaled in units of  $w_1$ ,  $w_0 = 1$ , x = $\lambda_0 T_1/(6\hbar)$ ,  $z=\sqrt{12+\lambda_0^2}$  and  $y=zT_1/(6\hbar)$ . This leads to  $U_{12}=0$  for  $y=n_0\pi$  where  $n_0$  is an integer. These frequencies correspond to exact dynamic freezing for  $w_0 = w_1$ ; however such freezing is not stable against variation of  $w_0$ . For a generic  $w_0 \neq w_1$ , we do not find any exact dynamic freezing for L=3. In contrast, for  $\lambda_0/w_1=1$  and  $\hbar\Omega_1/w_1\simeq 1.2$ , we find a sharp dip in  $U_{12}(T,0)$  which suggest a presence of approximate dynamic freezing. Remarkably, our numerical results for  $w_0 \neq w_1$  suggest that this dip persists for  $w_0 \leq w_1$ at same  $\Omega_1$ ; its breadth increases with decreasing  $w_0$  and leads to a complete flat curve consistent with Floquet flat band for  $w_0 = 0$ . This feature is shown in Fig. 7 where  $|U_{12}(T,0)|^2$ is plotted as function of  $\hbar\Omega_1/w_1$  for  $\lambda_0/w_1=1$  and several representative  $w_0$ . For increasing L, we numerically find that such a dip remains leading slow evolution and the corresponding dip in  $O_{22}^{\rm DE}$  and  $S_E$  discussed in the main text. However, the position of the dip shifts to slightly higher frequency  $\hbar\Omega_1/w_1 \simeq 1.4$ . This is a consequence of contribution of additional evolution channels for L > 3 and we have not

been able to understand this analytically.

### SYMMETRY OF THE MICROMOTION

In this section, we are going to provide a proof for a reflection symmetry of the drive protocol around  $t=T_1/2$  for  $w_0=0$ . We shall provide an explicit proof using the square pulse protocol; the proof for a generic protocol follows the same line of reasoning.

Consider a Hamiltonian

$$H_1(t) = f_1(t)\hat{O}_1 + f_2(t)\hat{O}_2$$
 (23)

where  $\hat{O}_{1(2)}$  are general operators. Let us also consider a square pulse protocol such  $f_1(t)$  has a period  $T_1$  and  $f_2(t)$  has a period of  $\nu T_1$ , where  $\nu$  is an integer; the amplitudes of these drives are taken to be  $f_{01}$  and  $f_{02}$  respectively. We also define the Hamiltonian

$$H(s_1, s_2) = f_{01}s_1\hat{O}_1 + f_{02}s_2\hat{O}_2 \tag{24}$$

where  $s_{1(2)} = \pm 1$ . For the square pulse protocol, the instantaneous Hamiltonian,  $H_1(t)$ , can always be written in terms of  $H(s_1, s_2)$ .

In what follows, we shall consider micromotion under the action of H(t). To this end, we first note that for  $t \leq T_1/(2\nu)$ , the evolution operator is given by

$$U_1(t,0) = e^{-iH(1,-1)t/\hbar} = \sum_{m^{+-}} e^{-i\epsilon_m^{+-}t/\hbar} |m^{+-}\rangle\langle m^{+-}|$$
(25)

where  $\epsilon_m^{+-}$  denote eigenenergies corresponding H(1,-1) and  $|m^{+-}\rangle$  are the corresponding eigenstates. Next, let us consider the evolution operator between  $T_1(1-1/\nu) \leq t \leq T_1$ . Defining  $x_0 = T_1/(2\nu\hbar)$  and  $\delta t = t - T_1(2\nu - 1)$ , we find that the evolution operator can be written as

$$U_{2}(t,0) = e^{-iH(-1,1)\delta t/(2\nu\hbar)}e^{-iH(-1,-1)x_{0}}....e^{-iH(-1,-1)x_{0}}e^{-iH(1,1)x_{0}}....e^{-iH(1,1)x_{0}}e^{-iH(1,-1)x_{0}}$$

$$= e^{-iH(-1,1)(t-T_{1}(2\nu-1))/(2\nu\hbar)}e^{-iH(1,-1)T_{1}/(2\nu\hbar)}$$
(26)

where in the last line we have used the fact  $H(s_1,s_2)=-H(-s1,-s2)$  so that the contributions from the intermediate exponential factors cancel pairwise. Noting that  $\epsilon_m^{s_1,s_2}=-\epsilon_m^{-s_1,-s_2}$  and  $|m^{s_1,s_2}\rangle=|m^{-s_1,-s_2}\rangle$  (up to an unimportant global phase), we find

$$U_{2}(t,0) = \sum_{m^{+-}} e^{-i\epsilon_{m}^{+-}T_{1}/(2\nu\hbar)} |m^{+-}\rangle\langle m^{+-}|$$

$$\times \sum_{m^{-+}} e^{-i\epsilon_{m}^{-+}(t-T_{1}(2\nu-1))/(2\nu\hbar)} |m^{-+}\rangle\langle m^{-+}|$$

$$= \sum_{m^{+-}} e^{-i\epsilon_{m}^{+-}(T_{1}-t)/\hbar} |m^{+-}\rangle\langle m^{+-}|$$

$$= U_{1}(T_{1}-t,0)$$
(27)

Thus, the evolution operator, for  $t \leq T_1/(2\nu)$ , is symmetric around  $T_1/2$ . A similar derivation can be carried out for any  $(m-1)T_1/(2\nu) \leq t \leq mT_1/(2\nu)$  and we find the symmetry  $U(t,0) = U(T_1-t,0)$  for all  $t \leq T_1/2$ . Since U controls

the evolution of all operator correlations and expectations, we find that the dynamics is symmetric around  $T_1/2$ . The same relation can also be derived for other protocols using a suitable Trotter decomposition of U.

- S. Moudgalya, A. Prem, D. A. Huse, and A. Chan, Phys. Rev. Res, 3, 023176 (2021).
- [2] L. D'Alessio and M. Rigol, Phys. Rev. X 4, 041048 (2014).
- [3] L. D'Alessio, Y. Kafri, A. Polkovnikov, and M. Rigol, Adv. Phys. 65, 239 (2016).
- [4] P. Das, D. S. Bhakuni, L. F. Santos, and A. Sharma Phys. Rev. A 108, 063716 (2023).
- [5] A. Sen, D. Sen, and K. Sengupta, J. Phys. Condens. Matter 33, 443003 (2021).
- [6] A. Soori and D. Sen, Phys. Rev. B 82, 115432 (2010).
- [7] T. Bilitewski and N. R. Cooper, Phys. Rev. A 91, 063611 (2015).
- [8] B. Mukherjee, S. Nandy, A. Sen, D. Sen, and K. Sengupta, Phys. Rev B 101, 245107 (2020).
- [9] B. Mukherjee, A. Sen, D. Sen, and K. Sengupta, Phys. Rev B 102, 075123 (2020).